Rotor5: Rotor analysis under 5 hours using ultra-fast and high-fidelity CFD simulation and automatic meshing

Runda Ji *, Feilin Jia †, Philippe Spalart ‡, and Zongfu Yu §
Flexcompute Inc, Belmont, Massachusetts, 02138

Qiqi Wang ¶
Massachusetts Institute of Technology, Cambridge, Massachusetts 02139
Flexcompute Inc, Belmont, Massachusetts, 02138

We introduce a novel workflow called Rotor5 to simplify and accelerate the traditional high-fidelity rotor simulations by integrating (1) CAD preparation (2) mesh generation and (3) CFD solver into an end-to-end process. We quantify the limitations of a popular low-fidelity rotor design tool called Xrotor and demonstrate the necessity of using a high-fidelity CFD solver such as Rotor5. Using both Xrotor and Rotor5, we investigate the tiltrotor XV-15 at two different flight conditions: (1) airplane propeller mode in forward flight and (2) helicopter hovering mode, where the fundamental limitations of low-fidelity Xrotor could cause a catastrophic design failure. A major cause for this is the tip vortex of the preceding blade.

I. Nomenclature

R	=	rotor disk radius
A	=	rotor disk area, πR^2
Ω	=	rotor angular speed
T	=	rotor thrust
Q	=	rotor torque
C_T	=	rotor thrust coefficient, $T/\rho(\Omega R)^2 A$
C_Q	=	rotor torque coefficient, $Q/\rho(\Omega R)^2 AR$
FoM	=	figure of merit, FoM=$\frac{C_T^{3/2}}{\sqrt{2}C_Q}$

II. Introduction

Low-cost tools such as Xfoil and Xrotor [1, 2] have been widely applied in rotor designs [3]. However, with the exception of XFOIL for pure airfoil cases, such tools are insufficiently accurate, which could mislead engineers into a wrong direction at the early stage of a design process. Without a high-fidelity CFD solver, the engineers won't be able to realize the error until they physically build the rotor and go through wind tunnel/fight tests, which are both money and time-consuming. Unfortunately, rotor engineers appear to be restricted to those inaccurate low-fidelity tools. This is because the traditional high-fidelity approaches are extremely time-consuming, involving lengthy processes of (1) CAD preparation (2) mesh generation and (3) unsteady CFD simulation. Sometimes, the traditional high-fidelity CFD approaches could be even more time-consuming than the wind tunnel/fight tests. In addition, their results come with an uncertainty that is not precisely known, linked to numerical errors and to physical-modeling errors; uncertainty also exists for ground tests.

In this article we introduce a novel workflow, coupled with a next-gen solver to provide high-fidelity CFD results with push-button ease of use and unprecedented speed. Once the geometric definitions (such as airfoil cross-sections and/or hub/fairing profiles) are input, the Engineering Sketch Pad (ESP) [4] automatically constructs a water-tight CAD geometry. Instead of creating the mesh manually, the system scripts and automates the meshing process via Glyph [5]. The automatically generated mesh, along with the mesh and solver configuration files, are uploaded to our cluster via Flow360 Python API and our cluster launches the cases/simulations instantaneously. Figure 1 illustrates the superiority of Rotor5 versus traditional high-fidelity CFD solvers.

*CFD Application Scientist
†CFD Research Scientist
‡Head of Fluid Mechanics
§Co-founder of Flexcompute
¶Associate Professor, Department of Aeronautics and Astronautics, MIT. Co-founder of Flexcompute

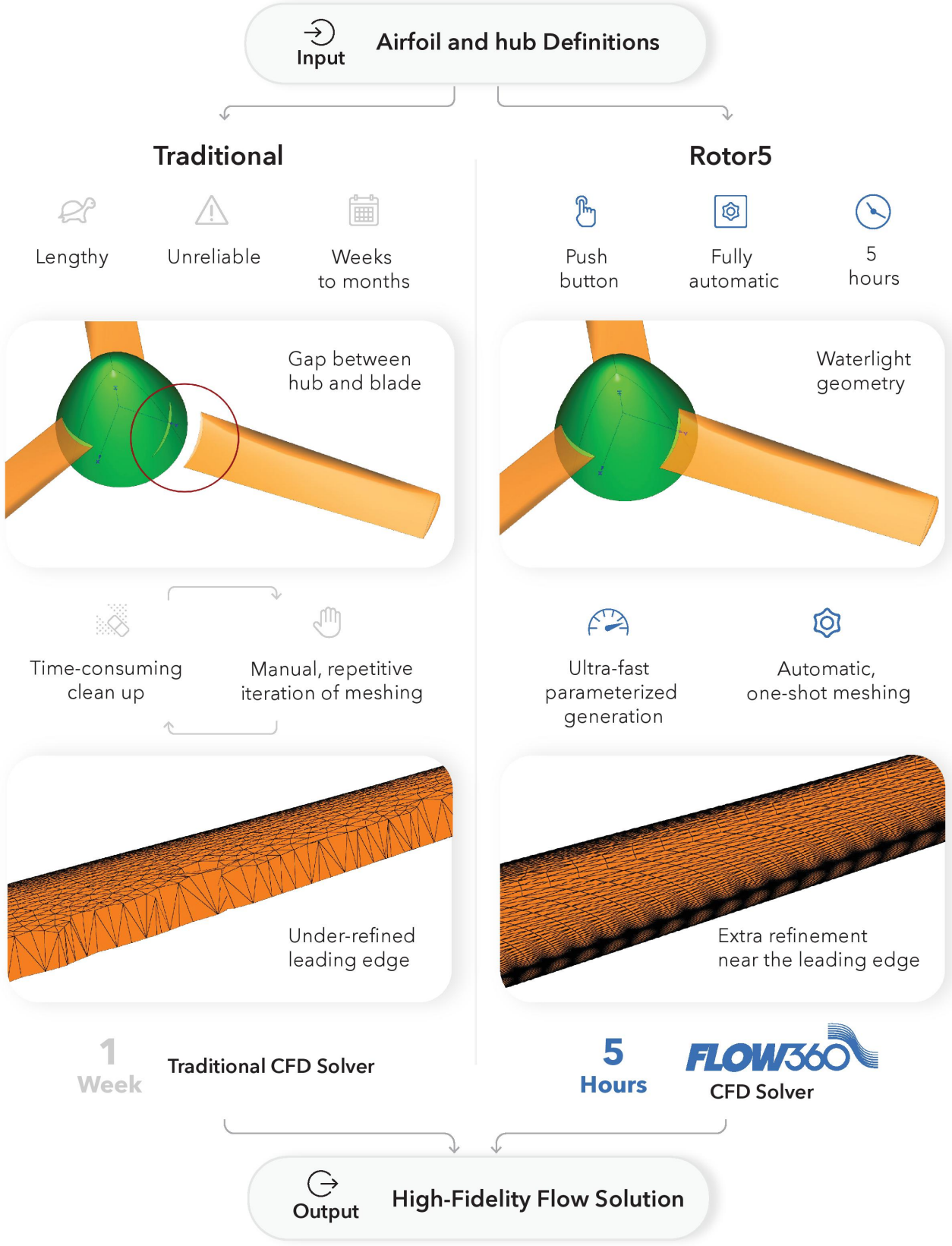

Fig. 1 Comparison between traditional high-fidelity CFD solvers and Rotor5. Time estimated based on a 35M-nodes mesh.

In figure 1, the gaps between the NURBS surfaces are exaggerated to illustrate a common issue in traditional CAD files, which is typically caused by problematic Boolean operations with loose tolerance. Instead of having a single loop shared by the hub and the blade, there are actually two loops saved in the CAD file, one defining the hole on the hub, the other defining the root of the blade. For traditional CAD files, the meshing tool will compute the distance between two edges. If the distance between the two edges are lower than a given tolerance, then these two edges will be considered as identical, i.e. degenerated into same edge. Otherwise, the meshing software will treat the edges separately and hence the nodes on the two edges will mismatch. In this scenario, the surface mesh eventually generated will not be watertight. So how do we eliminate this issue? In our approach, in addition to the definition of the NURBS surfaces, we also pass the topological information into the meshing tool, and hence we inherently know whether or not a pair of surfaces are connected or not and we will not have such spurious edges when generating the surface mesh.

Another common issue with the traditional approach is the NURBS surfaces are not correctly split. For a single NURBS surface, if there are two (or multiple) branches close to each other, it will be challenging for the meshing algorithm to figure out which branch to project the nodes on. Take the un-split leading edge for example, we can see self-intersecting cells near the leading edge, because the upper and lower surfaces of the blade are too close to each other. In our approach, since we are constructing the geometry from airfoil cross-sections, we inherently know the coordinate of the leading edge for each airfoil and we could easily spilt the blade into upper and lower surfaces. Additionally, an-isotropic layers near the leading edge are also automatically generated to further refine the surface mesh along the chord-wise direction.

III. Geometry and Flow Conditions

A. XV-15 Geometry

Table 1 Main properties

Parameter	Value
Number of blades, N_b	3
Rotor radius, R	150 inches
Reference blade chord, c_{ref}	14 inches
Aspect ratio, R/c_{ref}	10.71
Rotor solidify, σ	0.089
Linear twist angle, Θ	-40.25°

Table 2 Airfoil definitions

r/R	Airfoil
0.09	NACA 64-935
0.17	NACA 64-528
0.51	NACA 64-118
0.80	NACA 64-(1.5)12
1.00	NACA 64-208

For demonstration, we select tiltrotor XV-15 [6] as our example geometry. The CFD model of XV-15 rotor was generated based on the experiment by Felker [7]. The main geometric characteristics of the full-scale XV-15 rotor blades are listed in Table 1. The rotor blade consists of 5 NACA 6-series aerofoil sections, which are reported in Table 2.

B. Mesh

The volume mesh in this study is a multi-block unstructured mesh, which contains 2 layer and 5 blocks. Table 3 summarizes the key meshing statistics in those blocks

Table 3 Meshing parameters for the XV-15 rotor mesh [8].

Computational Domain	Number of Nodes
Farfield background	15.10M
Nearfield background	2.69M
Body-fitted mesh enclosing the blade	6.27M

As shown in figure 2a, the yellow cylinder represents the stationary farfield background, whereas the blue cylinder in the middle is the rotational nearfield background.

Since we want to simulate XV-15 tiltrotor with different blade collective angle, instead of re-generating the entire nearfield mesh for each collective angle, we further split the nearfield mesh into 4 sub-components. As illustrated in figure 2b, within the

blue nearfield background, there are 3 cylindrical body-fitted domains enclosing the blades. For different blade collective angles, we only need to rotate the red body-fitted domains respect to the pitching axis.

As depicted in figure 2c The axis of each cylindrical body-fitted domain is along the pitching axis of the enclosed blade. We only need to generate one body-fitted domain and the rest two body-fitted domains are simply duplicated. Before we start the unsteady simulations, The nearfield background and three body-fitted domains are merged together. While running the simulation, the merged nearfield mesh rotates whereas the farfield mesh remains stationary.

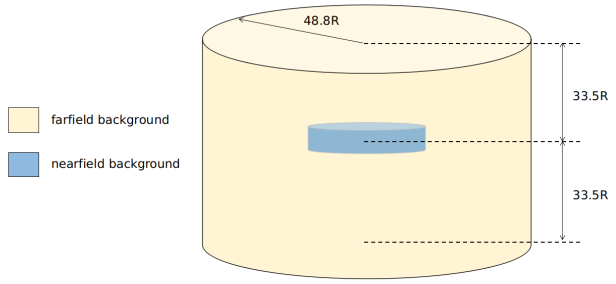

(a) Dimensions of the farfield background domain. Axial: $\pm 33.5R$ **above and below the rotor disk plane. Radial:** $48.8R$ **from the rotational axis.**

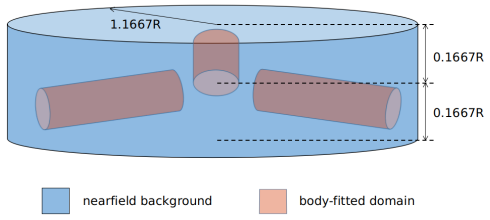

(b) Dimensions of the nearfield background domain. Axial: $\pm 0.1667R$ **above and below the rotor plane. Radial:** $1.1667R$ **from the rotational axis.**

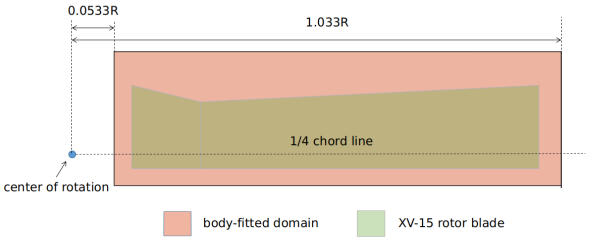

(c) Dimensions of the body-fitted domain. Span-wise: $0.1367R$ **to** $1.0333R$**. Radius of the cylinder:** $0.1024R$**.**

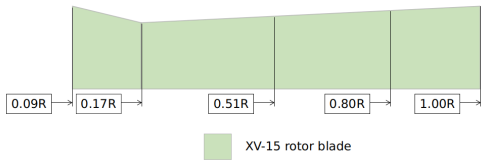

(d) Planform of the XV-15 rotor blade

Fig. 2 Sketch of the domains of farfield background, nearfield background and body-fitted for meshing and the Planform of the XV-15 rotor blade.

C. Flow Conditions

In order to quantitatively compare the accuracy between our high-fidelity Rotor5 versus the lower-fidelity Xrotor, we analyze XV-15's performance at two specific flight conditions: (1) airplane propeller mode in a forward flight and (2) helicopter hovering mode. The flow conditions are summarized in table 4.

Table 4 Flow conditions for the full-scale XV-15 tiltrotor blade.

	Airplane Mode	**Hover Mode**
Blade-tip Mach number (M_{tip})	0.54	0.69
Reynolds number (Re)	4.50×10^6	4.95×10^6
Blade pitch angle (θ_{75})	26°,27°,28°,28.8°	0°,3°,5°,10°,13°
Angle of attack (α)	-90°	
Advance ratio	0.337	

IV. Results and Discussion

A. Figure of Merit

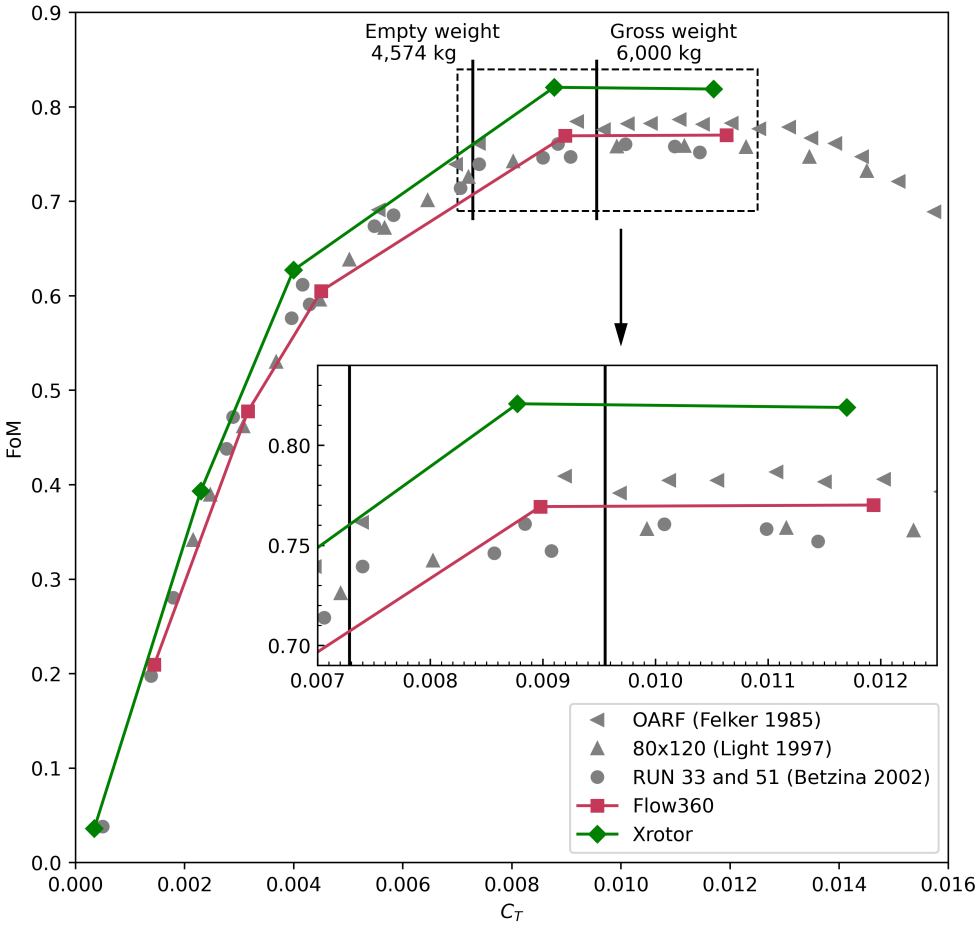

Fig. 3 Figure of merit (FoM) versus thrust coefficient (C_T) of hovering helicopter mode. Vertical lines show the hovering range of the XV-15 rotor.

Over-predicting the figure of merit (FoM) in helicopter mode is one of the limitations of Xrotor. The two vertical lines in figure 3 delimit the hovering range of the XV-15 rotor, between empty weight $W_{\text{empty}} = 4,574$ kg and maximum gross weight $W_{\text{gross}} = 6,000$ kg. [6] Since there are two rotors providing the thrust simultaneously, the thrust generated by each rotor is $T = \frac{1}{2}\, g\, W$, where $g = 9.8$ m/s^2. Recall the definition of the thrust coefficient C_T,

$$C_T \equiv \frac{T}{\rho(\Omega R)^2 A} = \frac{1}{2}\frac{g\, W}{\rho(\Omega R)^2 A} \tag{1}$$

Therefore,

$$C_{T\text{empty}} \approx 0.00728 \qquad C_{T\text{gross}} \approx 0.00955 \tag{2}$$

Within this critical range, Xrotor significantly over-predicts the FoM and hence unprepared engineers could be over-confident of their design. As summarized in table 5 the peak FoM predicted by Xrotor is much higher than the experimental measurements. In other words, given a fixed torque/power, the rotor is not generating as much thrust as Xrotor predicted, causing the aircraft not to meet the mission requirements during flight test.

Table 5 Peak FoM for the XV-15 rotor in the helicopter hovering mode.

	Experiments			CFD	
	Felker [7]	Light [9]	Betzina [10]	Flow360	Xrotor
Peak FoM	0.788	0.761	0.761	0.770	0.821

B. Blade-Vortex Interaction

Another critical limitation of the low-fidelity tools, such as Xrotor, is that they cannot predict the blade vortex interaction at low or zero advance ratio. As shown one the left of figure 4a, the freestream velocity is high enough in airplane mode, so the vortices generated by the previous blade are quickly washed downstream and hence there is essentially no blade-vortex interaction. However, for helicopter hovering mode depicted in figure 4b, the vortices from the previous blade will graze the next blade, causing a strong blade-vortex interaction that the low-fidelity Xrotor cannot predict. Even if an engineering correction were applied to the FoM, this means that the engineer has no handle on improvements to the structural design near the tip, whether through planform, droop, or twist.

Figure 4a is rich in aerodynamic lessons. First it displays some peculiarities of the Q-criterion. Although designed to identify vortices, it also takes high values in boundary layers over convex surfaces. Therefore, it fortuitously "shows" the blade; however there is a gap around 2/3 of chord, due to the curvature being lower. We, oddly, "see through the blade." Q-criterion is high again near the trailing edge. Note that these features in the figures are highly dependent on the level of Q-criterion chosen by the user.

Also notice in both figures the bands of Q-criterion emanating from the trailing edge around 20 and 55% of the blade radius, in addition to the expected tip vortex. We attribute this to the rectangular planform which raises circulation outboard and to blade twist and airfoil changes along the XV-15, causing circulation variations and therefore trailing vorticity. Further, a loading surge around 88% radius driven by the preceding vortex creates a small counter-rotating vortex, seen in figure 4b. Recall that this creates induced drag.

A tiltrotor design requires a severe compromise between the two flight modes, and accurate CFD combined with thorough flow visualization in both regimes is a must.

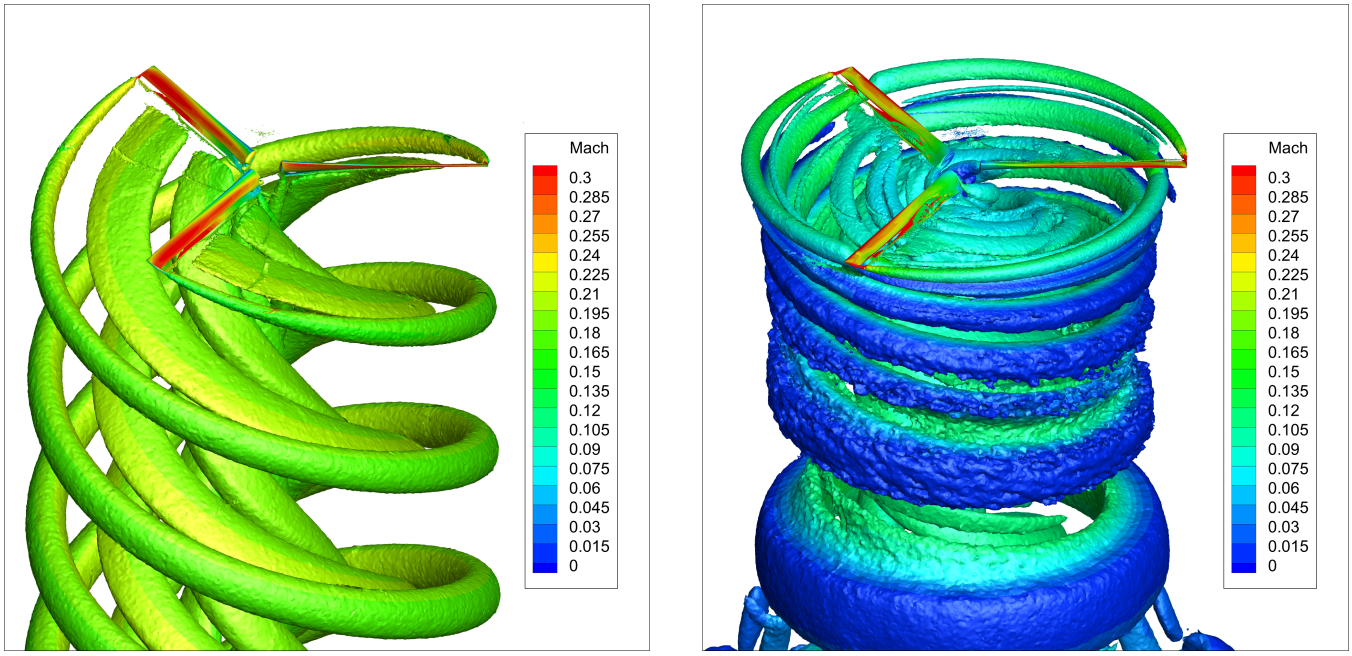

(a) Airplane mode with collective pitch angle $\theta_{75} = 28.8°$, advance ratio = 0.337.

(b) Hovering mode with collective pitch angle $\theta_{75} = 13°$

Fig. 4 Wake visualization using Q-criterion colored by Mach number.

As shown in figure 5, in airplane propeller mode in forward flight, the low-fidelity Xrotor is doing well in predicting sectional loading. However, in helicopter hovering mode, there is a significant difference between Xrotor and Flow360. This is especially the case near the tip of the blade where the blade-vortex interaction happens.

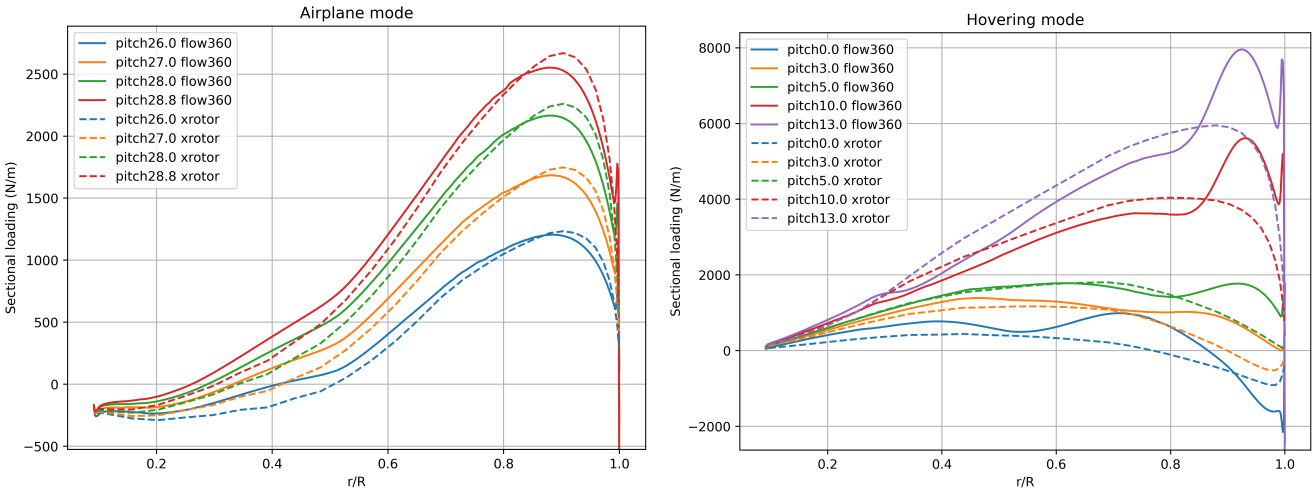

Fig. 5 Sectional loading on a blade. Left: airplane propeller mode. Right: helicopter hovering mode. Different colors represent to different blade pitching angles. Solid and dashed lines are Flow360 and Xrotor results, respectively.

C. Downstream Wake Comparison

In Xrotor, there are two pairs of axial and tangential velocities we need to distinguish: (VA,VT) and (VAslip, VTslip). (VA,VT) are the velocities on the blade, whereas (VAslip, VTslip) are "slipstream" velocities in the downstream wake, which we want to analyze. In addition to plotting the velocity distribution versus r/R, we could also plot the results versus the Stokes stream function ψ. The mass flux per area $\dot{m}(r)$ is defined as:

$$\dot{m}(r) = \frac{1}{2\pi}\int_0^{2\pi} \rho(r,\theta) v_a(r,\theta)\, d\theta \tag{3}$$

where $v_a(r,\theta)$ is the axial velocity. The stream function $\psi(r)$ can be further defined as:

$$\psi(r) = \int_0^{r} \dot{m}(r')\, 2\pi r'\, dr' \tag{4}$$

The total non-dimensional circulation on all blades at radius r is $B\Gamma(r)$, where B is the number of blades and $\Gamma(r)$ is the non-dimensional circulation on each blade (denoted as GAM in Xrotor). Specifically, the total non-dimensional circulation $B\Gamma(r)$ in Xrotor can be written as,

$$B\Gamma(r) = 2\pi \frac{r}{R} \frac{\overline{v}_t(r)}{V_\infty} \tag{5}$$

And hence the circumferentially-averaged tangential velocity $\overline{v}_t(r)$ is given by:

$$\overline{v}_t(r) = \frac{B\Gamma(r)}{2\pi r/R} V_\infty \tag{6}$$

Swirl $S(r)$ can be written as,

$$S(r) = \frac{1}{2\pi}\int_0^{2\pi} r v_t(r,\theta)\, d\theta = r\overline{v}_t(r) \tag{7}$$

Based on the equations above, we extracted and compared the axial velocity and swirl distribution predicted by Xrotor and Flow360.

1. Airplane Propeller Mode

Figure 6 and 7 show the circumferentially-averaged axial velocity versus r/R and stream function ψ, respectively. For XV-15 rotor in airplane propeller mode, the axial velocity profile predicted by Xrotor is reasonably good in general. The discrepancy near the root is primarily due to how we setup the hub radius in Xrotor i.e. XI0 in the *.prop file. In this paper, we set $R_{\text{hub}} = 0$ and Xrotor extrapolated the blade to $r/R \to 0$. However, if we set $R_{\text{hub}} = 0.09\ R$, then the axial velocity distribution for $r/R \in (0, 0.09)$ will be truncated off directly. In either way, we cannot obtain accurate axial velocity distribution near the root from Xrotor.

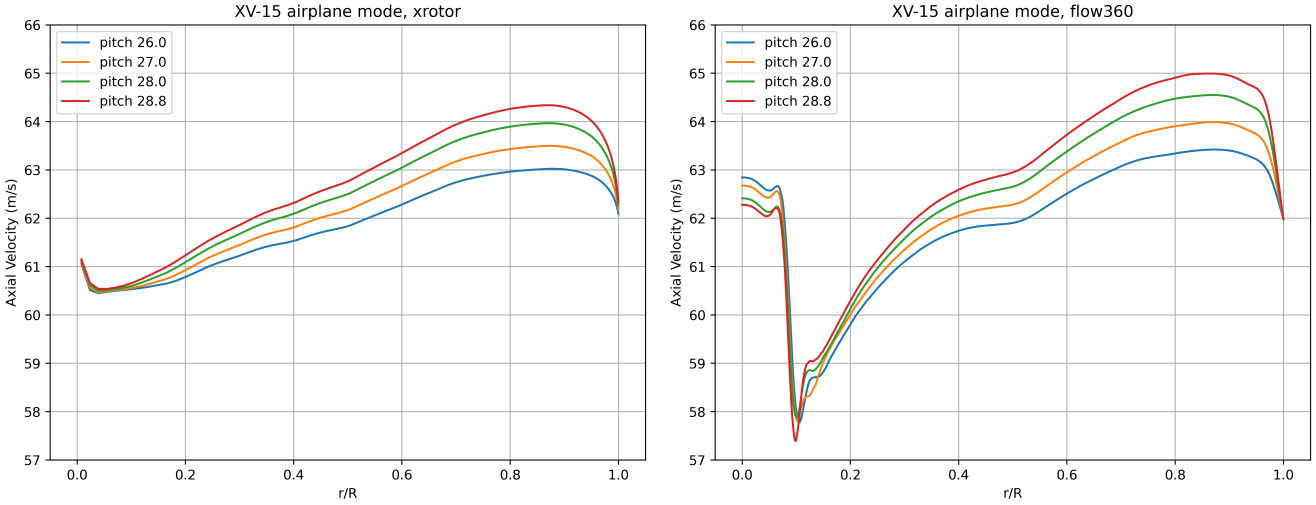

Fig. 6 Comparison of the axial velocity distribution just downstream of the propeller in airplane mode, plotting axial velocity versus r/R. Left: results predicted by Xrotor. Right: results predicted by Flow360.

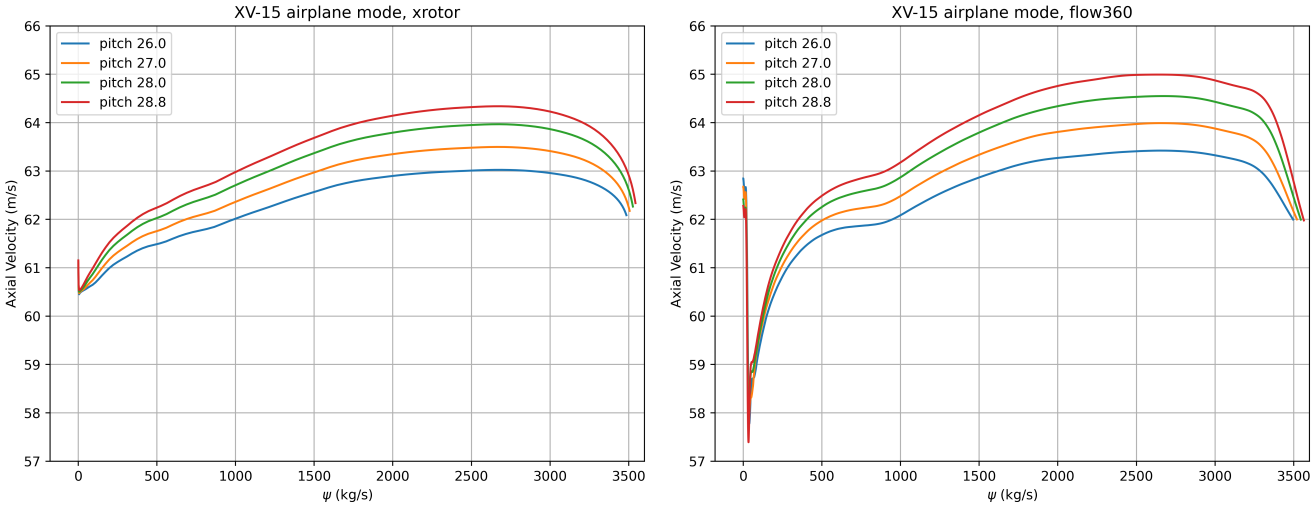

Fig. 7 Comparison of the axial velocity distribution just downstream of the propeller in airplane mode, plotting axial velocity versus stream function *psi*. Left: results predicted by Xrotor. Right: results predicted by Flow360.

The swirl versus r/R and stream function ψ are depicted in figure 8 and 9. For airplane mode with free-stream velocity along the axial direction, the swirl distribution predicted by Xrotor are fairly reasonable as well. However, similar to figure 6 and 7 we are still unable to extract accurate swirl distribution near the root from Xrotor.

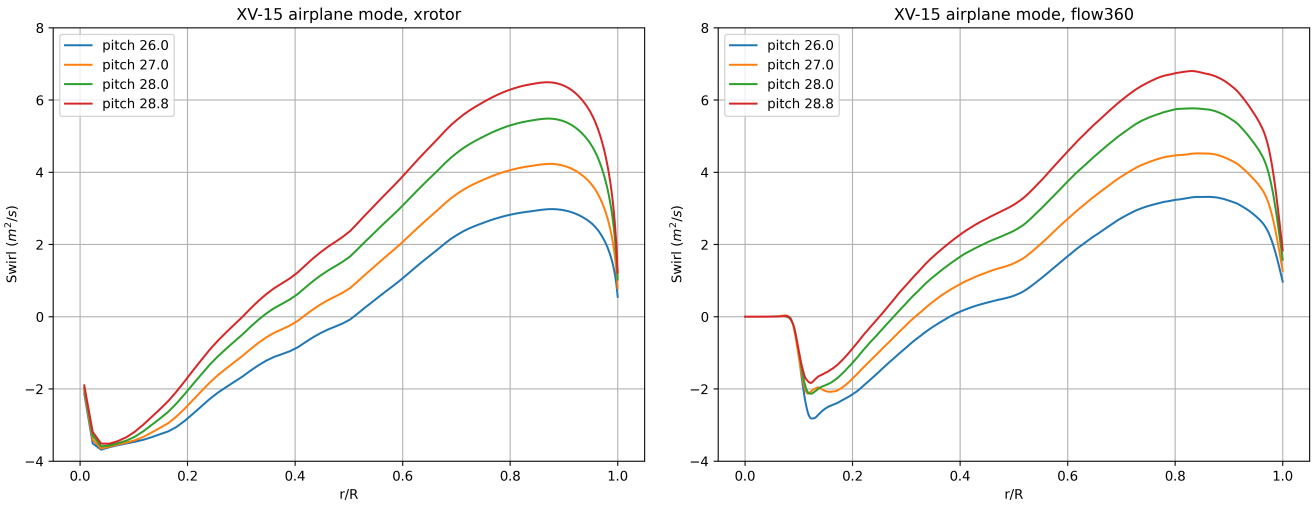

Fig. 8 Comparison of the swirl distribution just downstream of the propeller in airplane mode, plotting swirl versus r/R. Left: results predicted by Xrotor. Right: results predicted by Flow360.

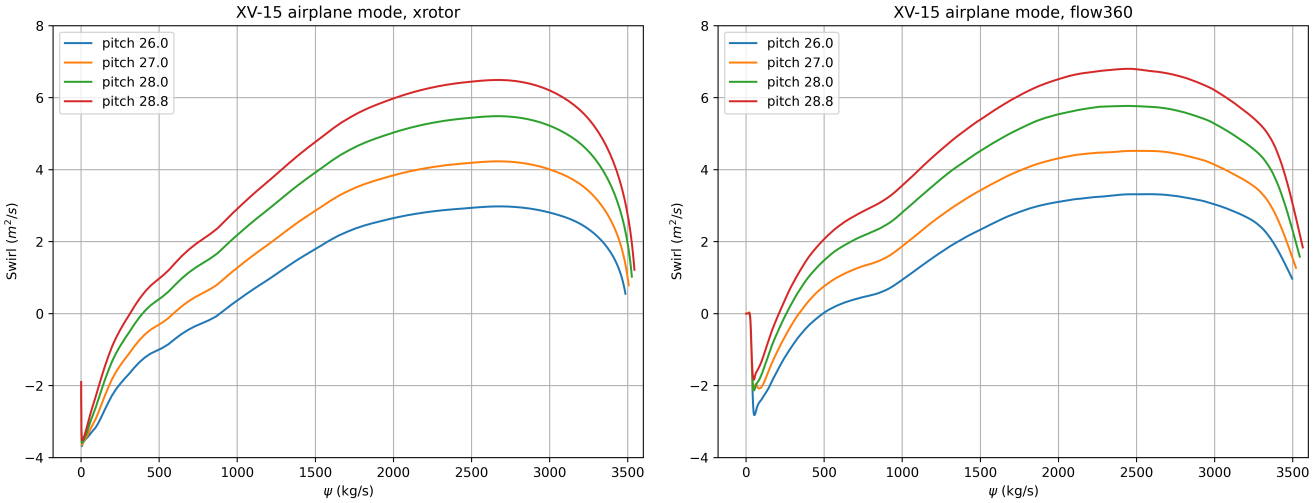

Fig. 9 Comparison of the swirl distribution just downstream of the propeller in airplane mode, plotting swirl versus stream function psi. Left: results predicted by Xrotor. Right: results predicted by Flow360.

2. Helicopter Hovering Mode

Figure 10 and 11 show the circumferentially-averaged axial velocity versus r/R and stream function ψ for XV-15 rotor in helicopter hovering mode. Compared to the airplane propeller mode, helicopter hovering cases are in general more challenging for Xrotor to accurately predict the flow field. Because there is no free-stream velocity flushing the vortex downstream and hence there is a strong blade-vortex interaction, which Xrotor cannot capture.

Within those hovering cases, lower pitching angle such as 0, 3 and 5 degrees are even more challenging than those cases with higher pitching angles. If we look at the axial velocity distribution, especially the region $r/R \in (0.4, 0.8)$, we can clearly see the induced axial velocity increases as the pitching angles increases, flushing away the tip vortex and suppress the blade-vortex interaction

It's worth noting that since the axial velocity is negative near the tip of the blade, the stream function is no longer monotonically increasing as r/R increases. Therefore, when plotting against ψ, we can see the "hooks" at the end of the curves.

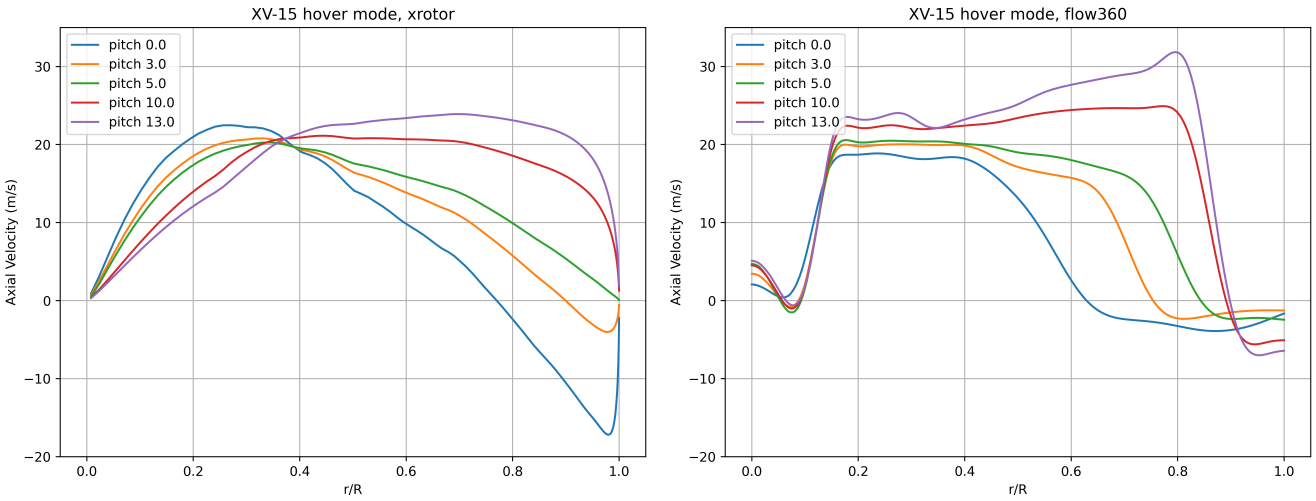

Fig. 10 Comparison of the axial velocity distribution just downstream of the rotor in helicopter hovering mode, plotting axial velocity versus r/R. Left: results predicted by Xrotor. Right: results predicted by Flow360.

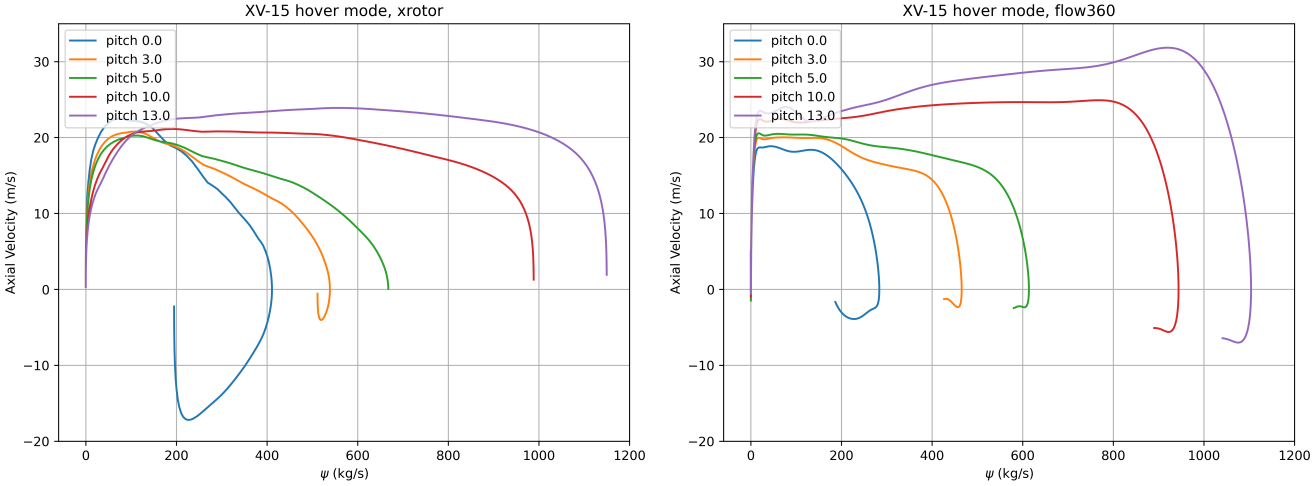

Fig. 11 Comparison of the axial velocity distribution just downstream of the rotor in helicopter hovering mode, plotting axial velocity versus stream function ψ. Left: results predicted by Xrotor. Right: results predicted by Flow360.

The swirl versus r/R and stream function ψ are depicted in figure 12 and figure 13, respectively. If we look at the swirl distribution predicted by Flow360, we can clearly see the "bumps" near the tip of the blades, particularly for pitching angle = 0 and 3 degrees, which are not captured by Xrotor. Recall the sectional loading distribution in figure 5 we can see the outer portion of the blade is very lightly loaded, which explains why the vortex sheet glides above the blades for almost 40% of the radius before turning downwards in figure 19.

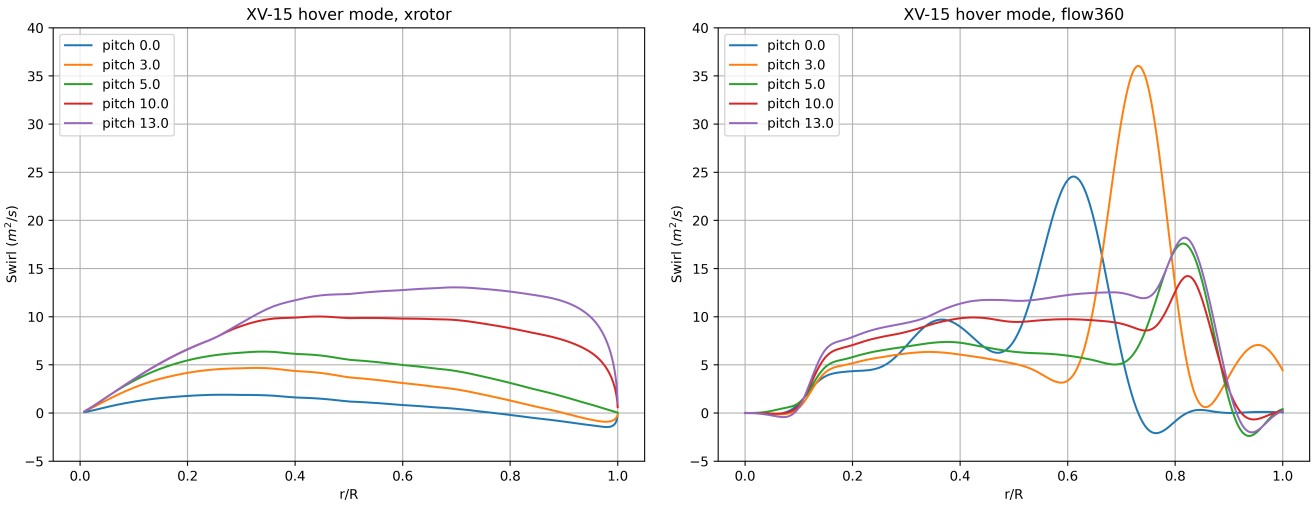

Fig. 12 Comparison of the swirl distribution just downstream of the rotor in helicopter hovering mode, plotting swirl versus r/R. Left: results predicted by Xrotor. Right: results predicted by Flow360.

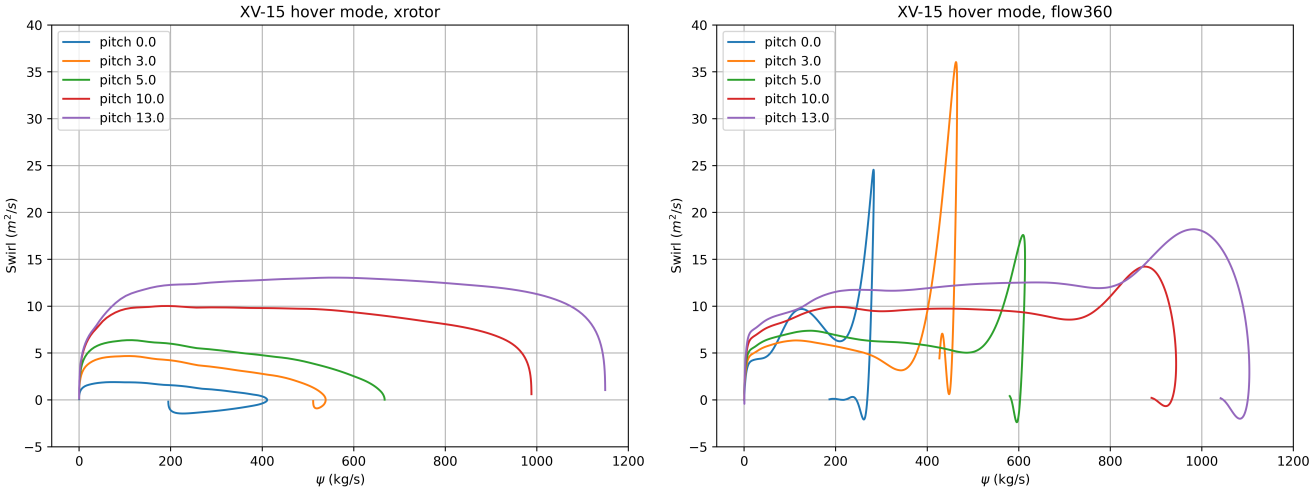

Fig. 13 Comparison of the swirl distribution just downstream of the rotor in helicopter hovering mode, plotting swirl versus stream function ψ. Left: results predicted by Xrotor. Right: results predicted by Flow360.

V. Future Work

A. Blade Element Theory

We are actively working on implementing blade element theory (BET) in Flow360. Some of the preliminary results from unsteady BET simulations are demonstrated in this section. Figure 14 and 15 show the downstream wake comparison of XV-15 rotor in airplane mode between Xrotor, Flow360 and the BET results, whereas figure 16 and 17 show the results for helicopter hovering mode. As shown in these figures, the axial velocity and swirl extracted from BET simulations are more accurate compared to Xrotor's prediction, which indicates the BET is an affordable alternative between low-fidelity Xrotor and high-fidelity full-rotor simulations.

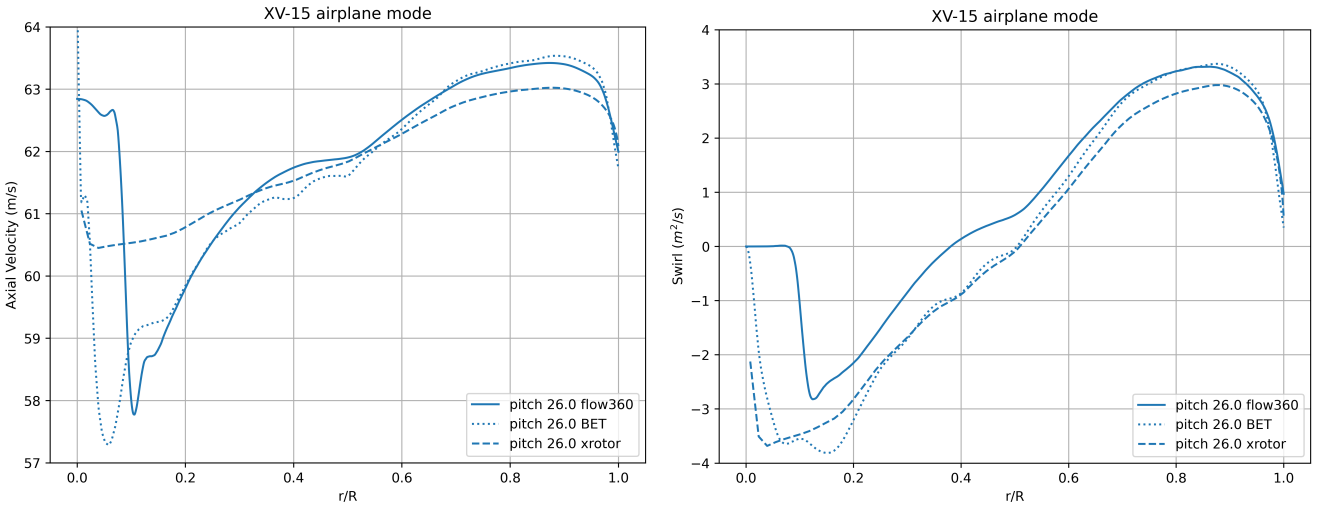

Fig. 14 Comparison of the wake just downstream of the propeller in airplane mode. Left: axial velocity versus r/R. Right: swirl versus r/R.

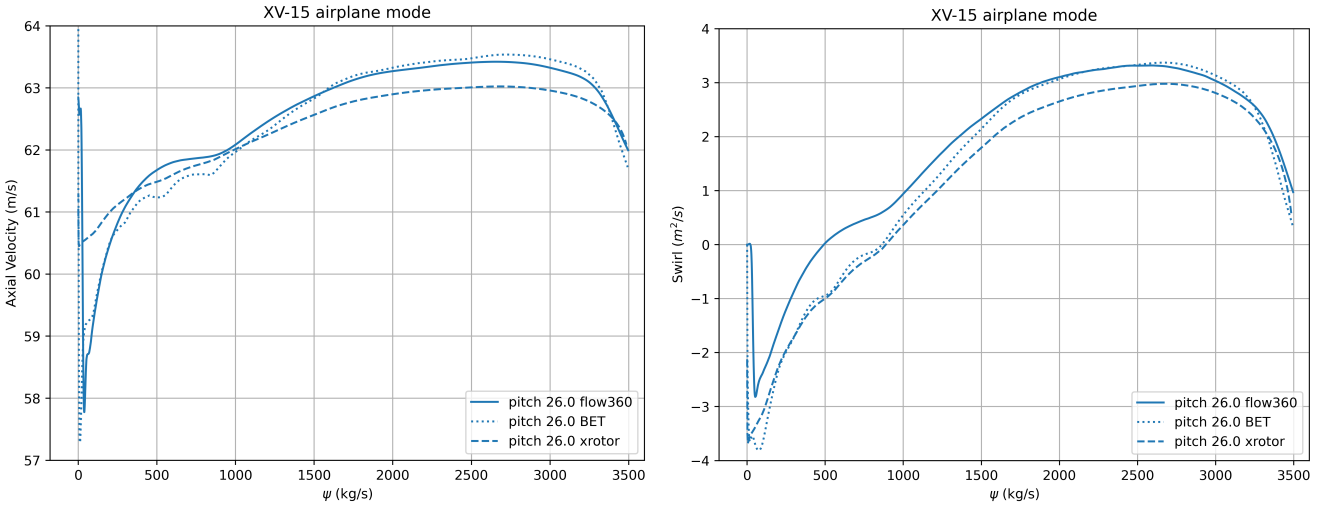

Fig. 15 Comparison of the wake just downstream of the propeller in airplane mode. Left: axial velocity versus stream function ψ. Right: swirl versus stream function ψ.

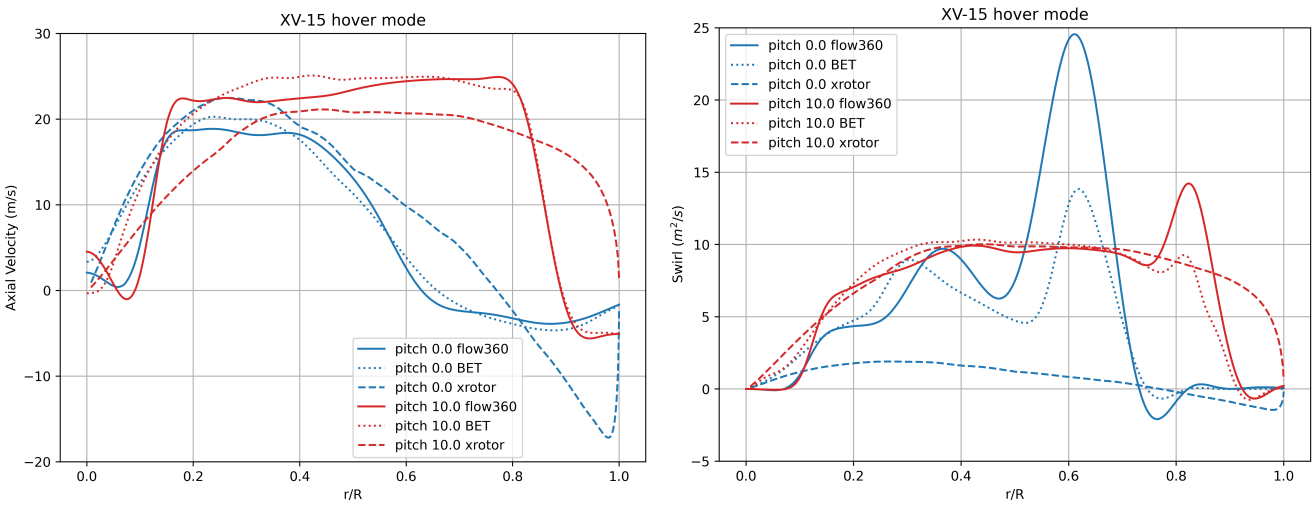

Fig. 16 Comparison of the wake just downstream of the rotor in airplane mode. Left: axial velocity versus r/R. Right: swirl versus r/R.

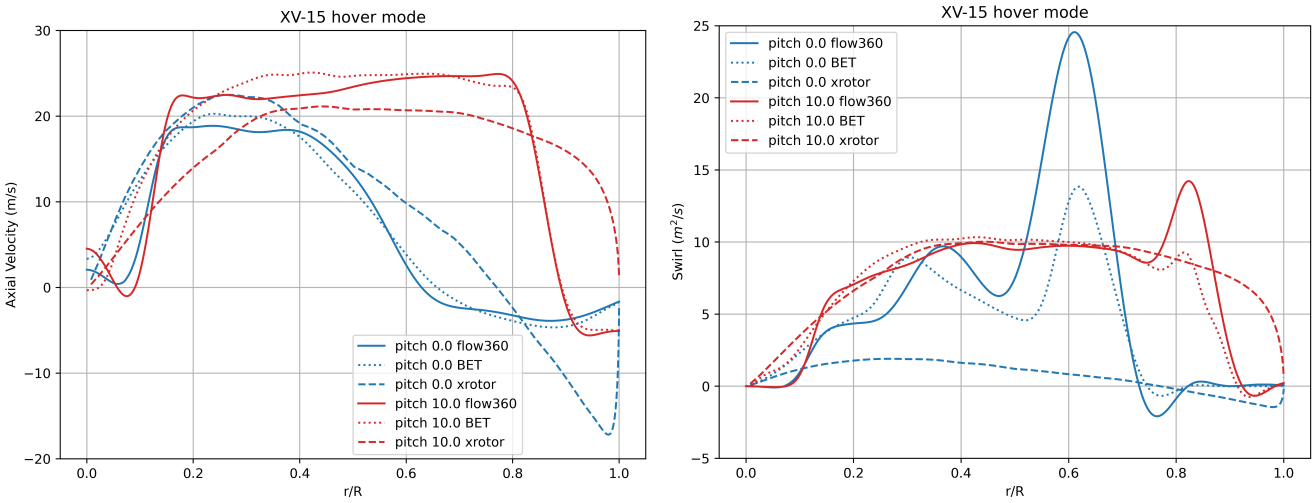

Fig. 17 Comparison of the wake just downstream of the rotor in airplane mode. Left: axial velocity versus stream function ψ. Right: swirl versus stream function ψ.

The Q-criterion comparison between full-rotor and unsteady BET simulations are depicted in figure 18, 19 and 20, where we can clear see the flow fields are qualitatively the same.

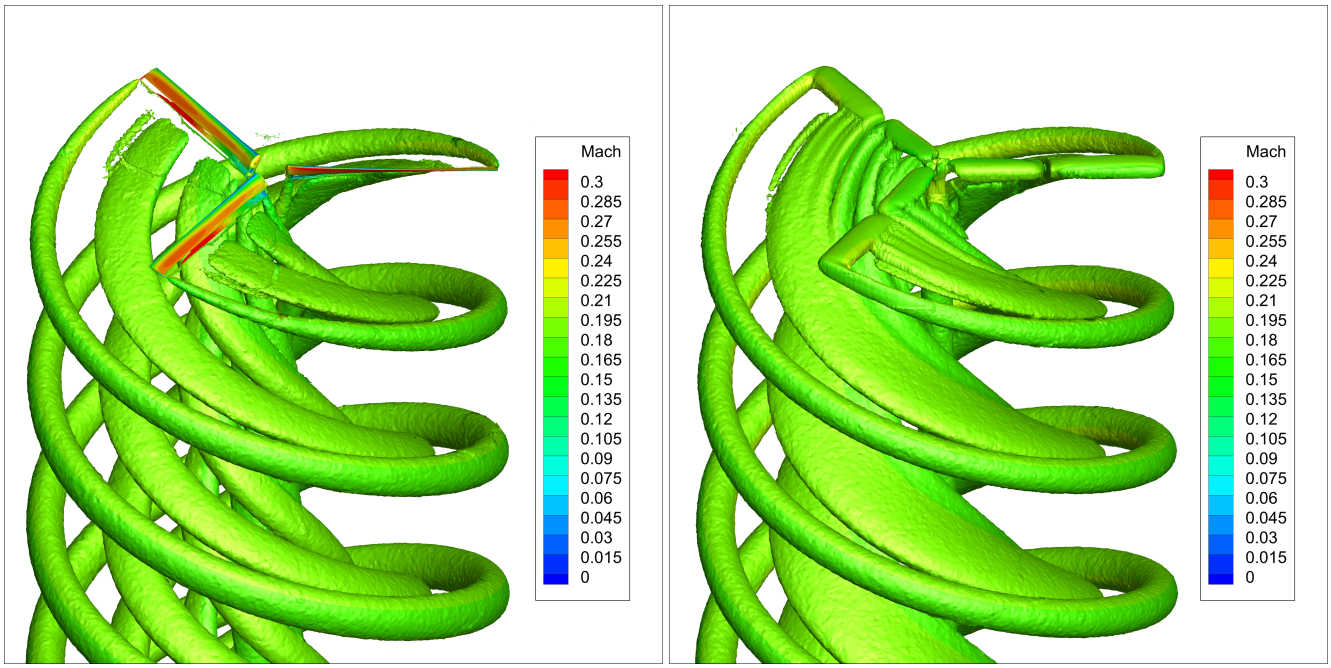

Fig. 18 Wake visualization using Q-criterion colored by Mach number, airplane mode, collective pitch angle $\theta_{75} = 26°$, advance ratio = 0.337. Left: full-rotor simulation. Right: blade element theory.

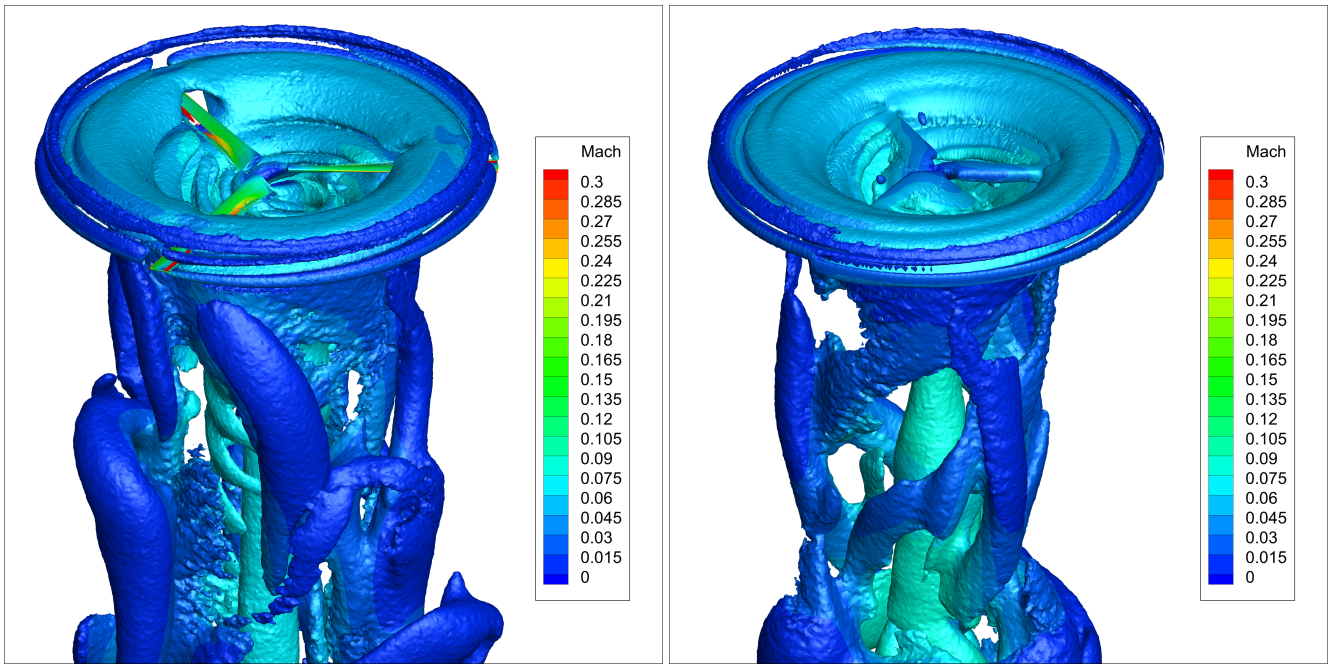

Fig. 19 Wake visualization using Q-criterion colored by Mach number, hovering mode, collective pitch angle $\theta_{75} = 0°$. Left: full-rotor simulation. Right: blade element theory.

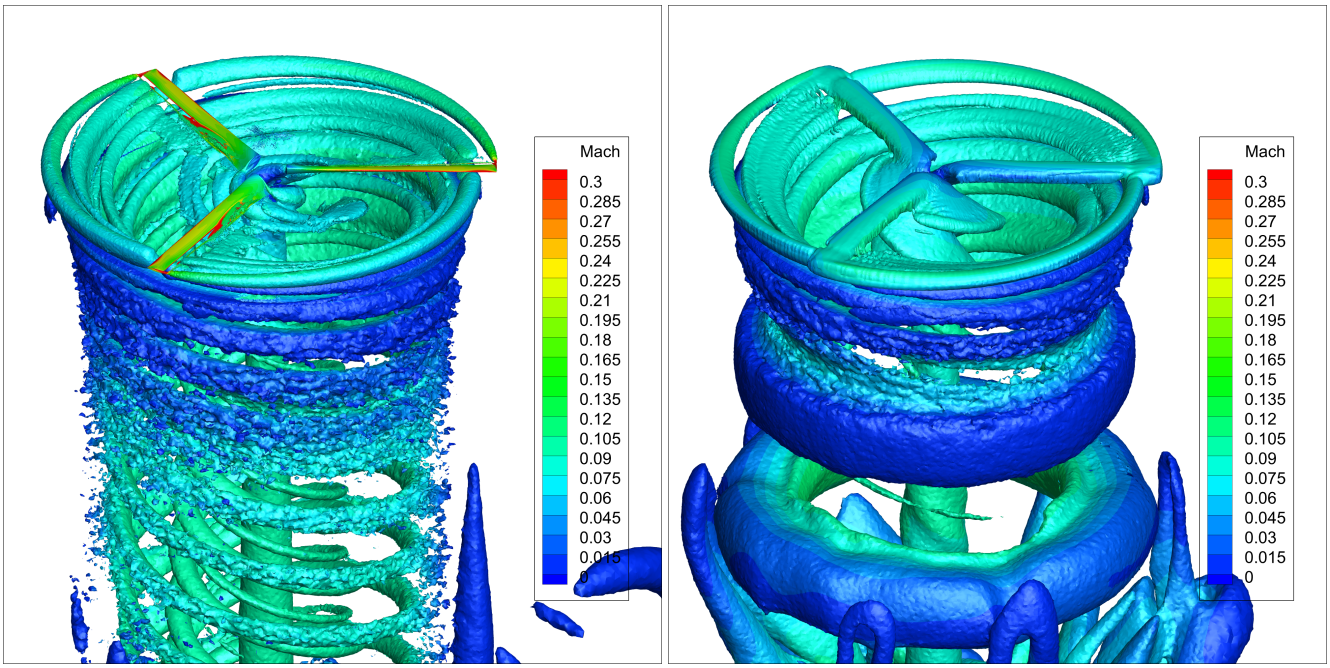

Fig. 20 Wake visualization using Q-criterion colored by Mach number, hovering mode, collective pitch angle $\theta_{75} = 10°$. Left: full-rotor simulation. Right: blade element theory.

VI. Conclusion

We introduced a novel workflow: Rotor5, which significantly simplified and accelerated the high-fidelity rotor simulation. Specifically, we integrated and/or automated (1) CAD preparation (2) mesh generation and (3) ultra-fast CFD solver, to provide our users high-fidelity CFD solutions with push-button simplicity and unprecedented speed.

In order to identify the limitations of low-fidelity tools, such as Xrotor, and demonstrate the benefits of using high-fidelity CFD solvers, we simulated tiltrotor XV-15 at two different flight conditions: (1) airplane propeller mode in a forward flight and (2) helicopter hovering mode. Although Xrotor could provide reasonable predictions at the airplane mode, it has two significant limitations when simulating the helicopter hovering mode: (1) over-predicting the figure of merit and (2) inability to resolve the blade-vortex interaction. There is no such limitations using our high-fidelity Rotor5, which is accurate, user-friendly and much faster than traditional high-fidelity solvers.

References

[1] Drela, M., "XFOIL: An analysis and design system for low Reynolds number airfoils," *Low Reynolds number aerodynamics*, Springer, 1989, pp. 1–12.

[2] Drela, M., and Youngren, H., "XROTOR download page," *Massachusetts Institute of Technology,[Online]. Available: http://web. mit. edu/drela/Public/web/xrotor/.[Accessed 27 6 2019]*, 2014.

[3] Alba, C., Elham, A., German, B. J., and Veldhuis, L. L., "A surrogate-based multi-disciplinary design optimization framework modeling wing–propeller interaction," *Aerospace Science and Technology*, Vol. 78, 2018, pp. 721–733.

[4] Haimes, R., and Dannenhoffer, J., "The Engineering Sketch Pad: A Solid-Modeling, Feature-Based, Web-Enabled System for Building Parametric Geometry," *21st AIAA Computational Fluid Dynamics Conference*, American Institute of Aeronautics and Astronautics, Reston, Virginia, 2013. https://doi.org/10.2514/6.2013-3073, URL http://arc.aiaa.org/doi/10.2514/6.2013-3073.

[5] Pointwise, I., "Glyph, Version 3.18.4," , Retrieved November 10, 2020. URL https://www.pointwise.com/glyph2/files/Glyph/cxx/GgGlyph-cxx.html.

[6] Maisel, M. D., Giulianetti, D. J., and Dugan, D. C., "The History of The XV-15 Tilt Rotor Research Aircraft: From Concept to Flight," *NASA Special Publication 4517*, 2000, p. 194.

[7] Felker, F., Young, L. E., and Signor, D., "Performance and Loads Data from a Hover Test of a Full-Scale Advanced Technology XV-15 Rotor," *Nasa Technical Memorandum 86-854*, , No. January 1986, 1986, p. 359.

[8] Jia, F., Moore, J., and Wang, Q., "Assessment of Detached Eddy Simulation and Sliding Mesh Interface in predicting Tiltrotor Performance in Helicopter and Airplane Modes," *AIAA AVIATION 2021 FORUM*, 2021, p. 2601.

[9] Light, J. S., "Results from an XV-15 rotor test in the national full-scale aerodynamics complex," *Annual Forum Proceedings - American Helicopter Society*, Vol. 1, No. May, 1997, pp. 231–239.

[10] Betzina, M. D., "Rotor Performance of an Isolated Full-Scale XV-15 Tiltrotor in Helicopter Mode," *American Helicopter Society Aerodynamics, Acoustics, and Test and Evaluation Technical Specialists Meeting*, 2002, pp. 1–12.